Comparative metaproteomics reveals functional differences in the blooming phytoplankton *Heterosigma akashiwo* and *Prorocentrum donghaiense*

Running title: Metaproteomes of the blooming phytoplankton

Hao Zhang,[a] Yan-Bin He,[b] Peng-Fei Wu,[a] Shu-Feng Zhang,[a] Zhang-Xian Xie,[a] Dong-Xu Li,[a] Lin Lin,[a] Feng Chen,[c] Da-Zhi Wang[a]

[a]State Key Laboratory of Marine Environmental Science/College of the Environment and Ecology, Xiamen University, Xiamen, 361005, China

[b]BGI-Shenzhen, Beishan Industrial Zone 11th building, Yantian District, Shenzhen, Guangdong 518083, China

[c]Institute of Marine and Environmental Technology, University of Maryland Center for Environmental Science, Baltimore, MD, USA

H.Z. and Y.H. contributed equally to this work.

*Corresponding author: Tel: +86 592 2186016, Fax: +86 592 2180655, e-mail address: dzwang@xmu.edu.cn (D.-Z. Wang)

KEYWORDS: phytoplankton bloom; formation mechanism; metaproteomics; nutritional niche

ABSTRACT

Phytoplankton blooms are natural phenomena in the ocean, which are the results of rapid cell growth of some phytoplankton species in a unique environment. However, little is known about the molecular events occurring during the bloom. Here, we compared metaproteomes of two phytoplankton *Heterosigma akashiwo* and *Prorocentrum donghaiense* in the coastal East China Sea. *H. akashiwo* and *P. donghaiense* accounted for 7.82% and 4.74% of the phytoplankton community protein abundances in the non-bloom sample, whereas they contributed to 60.13% and 78.09% in their individual blooming samples. Compared with *P. donghaiense*, *H. akashiwo* possessed significantly higher abundance of light-harvesting complex proteins, carbonic anhydrase and RuBisCO. The blooming *H. akashiwo* cells expressed more proteins related to external nutrient acquisition, such as bicarbonate transporter SLC4, ammonium transporter, nitrite transporter and alkaline phosphatase, while the blooming *P. donghaiense* cells highly expressed proteins related to extra- and intracellular organic nutrient utilization, such as amino acid transporter, 5'-nucleotidase, acid phosphatase and tripeptidyl-peptidase. The strong capabilities of light harvesting, as well as acquisition and assimilation of inorganic carbon, nitrogen and phosphorus facilitated the formation of the *H. akashiwo* bloom under the high turbidity and inorganic nutrient sufficient condition, whereas the competitive advantages in organic nutrient acquisition and reallocation guaranteed the occurrence of the *P. donghaiense* bloom under the inorganic nutrient insufficient condition. This study highlights the powerfulness of metaproteomics for revealing the underlying molecular behaviors of different co-existing phytoplankton species, and advances our knowledge on the formation of phytoplankton blooms.

IMPORTANCE

A deep understanding of the mechanisms driving bloom formation is the prerequisite for effective bloom management. Metaproteomics was applied in this study to reveal the adaptive and responsive strategies of two co-existing phytoplankton species *H. akashiwo* and *P. donghaiense* during their bloom periods. Metabolic features and niche divergence in light-harvesting, as well as carbon, nitrogen and phosphorus acquisition and assimilation likely promoted the bloom occurrence under

52 different environments. The molecular behaviors of co-existing bloom-causing species will give
53 clues to bloom monitoring and management in the oceans.

Applied and Environmental Microbiology

INTRODUCTION

Phytoplankton blooms are seasonal natural phenomena in the ocean, and are generally associated with physical, chemical and biological factors (1–3). Of particular importance are the harmful algal blooms (HABs), which involve toxic or otherwise harmful phytoplankton species and have become a global concern due to their negative impacts on the ecosystems, economics and public health (4–6). In the past few decades, the frequency, intensity and geographic distribution of HABs have increased dramatically due to the influences of anthropogenic activities and climate change (7–11). The formation of HABs derived from specific species can occur periodically within a unified environment (2, 5, 12). However, to date, the underlying molecular mechanisms that drive bloom formation remain poorly understood.

Light availability, dissolved CO_2 and nutrient resources are the most important environmental factors that affect bloom progression owing to their essential roles in regulating cell growth and proliferation. Moreover, the ability to acquire light, CO_2 and nutrients heavily influence bloom formation of different phytoplankton species. Light availability, nutrient composition, concentration and ratio have been reported to trigger bloom occurrence and succession of dinoflagellate, diatom, green algae and cyanobacteria in the global estuaries (13–16). Carbon acquisition efficiency varies greatly among phytoplankton species, and the carbon starvation caused by rapid consumption of high biomass partially affects the duration of bloom persistence (17, 18). Contrast to co-existing species, novel xanthorhodopsin-based light harvesting systems, efficient carbon concentrating and dissolved organic nutrient acquiring mechanisms facilitate bloom occurrence of some dinoflagellates (19–24). These studies demonstrate the close causal relationship between bloom occurrence and the surrounding conditions. However, little is known about the cellular metabolic responses of specific species to ambient environmental changes during the bloom.

Molecular-level approaches, such as taxon-specific meta-omics have been increasingly applied to exploring the metabolic capacity of HABs-forming species (25, 26). Ecogenomic approaches reveal the genetic advantages that facilitate the bloom of *Aureococcus anophagefferens* in environment with high levels of organic matter, metal and turbidity (27). Metatranscriptomic approaches provide

new insights into the gene response and resource redistribution of cells during natural phytoplankton blooms and the blooms simulated by iron and deep-sea water (24, 28–31). Comparative proteomics reveals that different light harvesting ability, nutrient assimilation mechanism and chemically mediated competition are partially responsible for the occurrence of nature and laboratory-simulated phytoplankton blooms (32-34). These studies shed light on the potential molecular mechanisms involved in the formation of HABs, and the discovery of the molecular behaviors of co-existing phytoplankton species within a unified environment have improved our understanding of the formation mechanisms of phytoplankton blooms.

The coastal East China Sea (ECS) is a highly eutrophic zone characterized by frequent-occurrence of HABs in the past few decades (35). Long-term field investigations have revealed that *Prorocentrum donghaiense*, *Heterosigma akashiwo* and other phytoplankton species cause extensive blooms from spring to early summer in this area (7, 36, 37). Similar bloom events and distinct ecological niches of these HABs species have also been reported in other coastal areas (38-41). However, the mechanisms that drive bloom occurrence of different phytoplankton species are unclear. Studies suggest that different ecological niches, as well as nutrient utilization and light-harvesting abilities among phytoplankton species might play important roles in bloom formation. In this study, we applied a metaproteomic approach to investigate the global protein expression profiles of two co-existing phytoplankton species *H. akashiwo* and *P. donghaiense* during their bloom periods, and characterized the differentially expressed proteins. Our results indicated different light-harvesting ability and nutritional niche divergence in utilization of carbon, nitrogen and phosphorus drove bloom occurrence of the two phytoplankton species under different ambient conditions.

RESULTS

Variations of chlorophyll a (Chl *a*) and nutrients during the bloom periods. The bloom processes of two co-existing phytoplankton species *H. akashiwo* and *P. donghaiense* were traced in the coastal ECS from May 1 to 21, 2014 (Fig. 1 and 2). In the first two days (May 1 to May 2), very

low cell densities of *H. akashiwo* and *P. donghaiense* were detected at each station of Za and Zb transects. Cell density of *H. akashiwo* increased at station Za3 from May 2 and then started to bloom radially and spread rapidly to the investigation area, covering transects Za and Zb. At station Za3, Chl *a* concentration increased from 2.82 to 6.3 μg/L from May 2 to 7, peaked around 9.67 μg/L on May 9, and then dropped to 1.96 μg/L on May 12. During the blooming period of *H. akashiwo*, *P. donghaiense* cells were almost undetected. At the end of the *H. akashiwo* bloom, cell density of *P. donghaiense* increased quickly from May 13 and began to bloom radially at station Zb7 (Fig. S1). Chl *a* concentration increased from 2.54 to 6.2 μg/L from May 13 to 21 at station Zb7.

Blooming phytoplankton cells rapidly consumed nutrients of surface seawater, and a negative correlation between the concentrations of inorganic nutrients and Chl *a* was observed. Before the *H. akashiwo* bloom, the concentrations of nitrate, ammonia and phosphate were 26.99, 5.3 and 1.34 μM at station Za3 on May 2, and then changed to 19, 7.54 and 0.03 μM on May 7. In the dissipation phase of *H. akashiwo* bloom, the concentrations of nitrate, ammonia and phosphate were 7.59, 3.09 and 0.04 μM on May 12. During the bloom period of *P. donghaiense*, the initial concentrations of nitrate, ammonia and phosphate were 15.68, 5.8 and 0.11 μM on May 13, and then changed to 2.5, 3.47 and 0.21 μM on May 21.

Overview of metaproteomics and phytoplankton community structure. Three phytoplankton samples representing the non-bloom (NB), blooming *H. akashiwo* (BHA) and blooming *P. donghaiense* (BPD) phases were selected for metaproteomic analysis. A total of 310084±31857, 327175±71775 and 451063±26774 MS/MS spectra were generated from the NB, BHA and BPD samples, respectively. Using the combined sequence dataset, 2.45±0.23%, 8.6±1.32% and 5.22±0.60% of the MS/MS spectra led to the identification of 9446 high-confidence proteins (Table S1). Among them, 6263, 6707 and 7566 proteins were detected in the NB, BHA and BPD samples, respectively. Specifically, 1542, 2244 and 1343 Ochrophyta proteins comprised 11.9%, 63.01% and 1.75% of the total community protein abundance; 3436, 3278 and 5073 Dinophyta proteins accounted for 15.74%, 20.85% and 92.11% of the total abundance; 317, 301 and 252 Bacillariophyta proteins constituted 7.44%, 1.48% and 0.96% of the total abundance; 196, 145 and 169 Cryptophyta proteins contributed

135 to 33.26%, 2.4% and 1.35% of the total abundance. Other phytoplankton groups, such as
136 Chlorophyta, Ciliophora and Haptophyta, represented relatively small and stable proportions in the
137 three samples (Fig. 3A and 3B).

138 The taxonomic composition of the 18S rDNA gene sequences also supported the metaproteomic
139 results (Fig. 3C). Ochrophyta comprised 1.53%, 63.26% and 0.74% of all community OTUs
140 abundances in the NB, BHA and BPD samples, respectively; Dinophyta comprised 64.48%, 33.24%,
141 89.79% of the total abundance; Bacillariophyta comprised 3.40%, 0.18%, 0.86% of the total
142 abundance; Cryptophyta comprised 4.22%, 0.23% and 0.14% of the total abundance, followed by
143 Chlorophyta, Ciliophora and Haptophyta, which accounted for only 1.73%, 0.90% and 1.82%.

144 **Major biological processes in the blooming species.** A total of 2152 *H. akashiwo* proteins and
145 3629 *P. dongaiense* proteins were detected in the three samples. In detail, the NB, BHA and BPD
146 samples contained 1461, 2150 and 1274 *H. akashiwo* proteins and 2350, 2171 and 3619 *P.*
147 *dongaiense* proteins, respectively (Fig. 3A, Table S2). Regarding protein abundance, *H. akashiwo*
148 contributed to 7.82%, 60.13% and 1.35% in the NB, BHA and BPD samples while *P. dongaiense*
149 accounted for 4.74%, 2.19% and 78.09% (Fig. 3B). Proteins related to cell growth and energy
150 metabolism were highly expressed in the two blooming species (Fig. 4A, Table S3). For *H.*
151 *akashiwo*, proteins related to carbon metabolism, ribosome, photosynthesis, photosynthesis-antenna
152 proteins, oxidative phosphorylation, biosynthesis of amino acid and glycolysis/gluconeogenesis were
153 most abundant in the NB, BHA and BPD samples. For *P. donghaiense*, proteins related to ribosome,
154 spliceosome, photosynthesis, carbon metabolism, oxidative phosphorylation, protein processing in
155 endoplasmic reticulum, biosynthesis of amino acid and photosynthesis-antenna proteins were most
156 abundant in the NB, HBA and BPD samples.

157 To minimize biomass and/or activity interferences among different bloom phases, the comparison
158 of the two species within the NB sample and the comparison between *H. akashiwo* in the BHA
159 sample and *P. donghaiense* in the BPD sample were performed (Fig. 4B, Table S3). As a result,
160 proteins related to nucleotide excision repair, carbon metabolism, carbon fixation, carotenoid
161 biosynthesis, vitamin B6 metabolism, glutathione metabolism, photosynthesis, oxidative

phosphorylation and photosynthesis-antenna proteins from *H. akashiwo* occupied higher proportions than those from *P. donghaiense* in the NB sample. Between the two blooming samples, proteins involved in carbon metabolism, carbon fixation, photosynthesis-antenna proteins, photosynthesis, nitrogen metabolism, oxidative phosphorylation, biosynthesis of N-glycan, carotenoid and fatty acid, glycolysis/gluconeogenesis, thiamine and glycerolipid metabolism from *H. akashiwo* in the BHA sample accounted for greater proportions in comparison with those from *P. donghaiense* in the BPD sample. Correspondingly, proteins involved in ABC transporters, protein export, spliceosome, lysosome, phagosome, galactose metabolism, two-component system, endocytosis, pyruvate metabolism, starch and sucrose metabolism from *P. donghaiense* in the BPD sample constituted greater proportions than those from *H. akashiwo* in the BHA sample.

DISCUSSION

Much attention has been focused on phytoplankton blooms, and the biotic and abiotic factors stimulating the bloom formation have been studied extensively (5, 8, 9, 28, 30). However, the metabolic features of various co-existing phytoplankton species during the bloom period remain poorly understood. In this study, we quantitatively compared protein expression levels of two bloom-causing phytoplankton species *H. akashiwo* and *P. donghaiense* at their blooming phase. Our data revealed remarkable differences in metabolic features that likely promote bloom formation, especially in the metabolic processes related to light harvesting and nutrient utilization (Fig. 7).

Light utilization. Marine phytoplankton rely on light to fix CO_2 into organic carbon, and light availability heavily affects the photosynthetic efficiency of phytoplankton. Therefore, the light-harvesting ability is an important determinant of phytoplankton growth and proliferation in the ocean. Light-harvesting complex (LHC) proteins bind antenna chlorophyll and carotenoid pigments that augment the light-capturing capacity of phytoplankton (42). A greater number of gene copies of LHCs in a HAB species is considered as a genetic advantage that facilitates its dominance among the co-existing species under a highly turbid estuary (27). Higher abundances of light-harvesting complex I chlorophyll a/b binding protein 1 (LHCA1), LHCA4, light-harvesting complex II

chlorophyll a/b binding protein 3 (LHCB3) and LHCB5 from *H. akashiwo* were detected than that from *P. donghaiense* during the bloom period, especially in the NB sample (Fig. 5A). This finding indicated stronger light-harvesting ability of *H. akashiwo*. The coastal ECS is characterized by high turbidity, and the intensity of photosynthetically active radiation attenuates rapidly with increasing water depth (43). The high expression level of LHC proteins in *H. akashiwo* may be an adaptive response to the high turbidity of coastal ECS, enabling it to outcompete other co-existing phytoplankton species, and thus facilitating its bloom under conditions of high turbidity. Correspondingly, *H. akashiwo* exhibits optimal growth rate over a wide light intensity range of 100-600 μmol photons m^{-2} s^{-1} (44). Moreover, it has been reported that the cellular chloroplast number of *H. akashiwo* can be adjusted for adaptation to varying light intensities (45).

The high cell biomass during phytoplankton blooms significantly attenuates light intensity in the water column. The *P. minimum* bloom causes a greater than six-fold increase on light diffuse attenuation coefficient and limits the average growth depth of phytoplankton from 1 m to 0.5 m (46). In our study, both *H. akashiwo* and *P. donghaiense* blooming cells highly expressed LHC proteins for the maximum light acquisition to cope with decreasing light availability (Fig. 5). Higher expression of LHC genes in the *H. akashiwo* and *P. donghaiense* blooming cells relative to their non-bloom cells is also detected (24-37). Abundance of LHC proteins from the *in situ* early-blooming cells of a dinoflagellate *Scrippsiella acuminate* is higher than that from the late-blooming cells, which is mainly caused by lower division rate of the late-blooming cells under severe nutrient starved condition (34). Degradation of LHCs is a vital responsive strategy to adapt to nutrient starvation which provides a nutrient source for other essential metabolic processes to maintain growth (47, 48). Taken together, *H. akashiwo* and *P. donghaiense* possessed strong abilities to adjust expression of LHC proteins to adapt to the varying ambient condition during the bloom period.

Carbon acquisition and fixation. The concentration of dissolved inorganic carbon (DIC) is a vital yet undervalued factor affecting the growth of phytoplankton in marine environment. DIC availability has been reported to influence the formation and distribution of phytoplankton species

(17, 49). The DIC in seawater comprises the sum of the relatively constant concentrations of HCO_3^- and CO_3^{2-} and the variable concentration of CO_2. The CO_2 in surface seawater is partially starved due to its sub-saturating concentration for phytoplankton ribulose-1,5-bisphosphate carboxylase/oxygenase (RuBisCO) affinity (50). This limitation is exacerbated by RuBisCO's oxygenation activity that competes with carboxylation, leading to the dissipation of fixed carbon (51).

Almost all marine phytoplankton species have evolved carbon concentrating mechanisms (CCMs) to enrich CO_2 at the catalytic site of the enzyme RuBisCO (52). As the key enzyme in CCMs, carbonic anhydrase (CA) facilitates the extra- and intercellular conversion between HCO_3^- and CO_2 (53). The existence of CCMs in *H. akashiwo* has been questioned, as previous studies failed to detect CA activity under different DIC-limitation conditions (54, 55). In the present study, higher proportions of intercellular CA, CA-alpha, CA-beta and CA-gamma from *H. akashiwo* were detected in the BHA sample than the NB and BPD samples (Fig. 5B), indicating that *H. akashiwo* possessed CCMs that allow adaptation to ambient DIC changes. Multiple types of CA have also been reported in a metatranscriptome study (37). Compared with *H. akashiwo*, only very small proportions of CA and CA-delta from *P. donghaiense* were detected in the three samples. Moreover, CA and CA-delta from *P. donghaiense* were higher expressed in the BHA and BPD samples than that in the NB sample (Fig. 5B). A previous metatranscriptomic study reveals significant increase of two CA-delta genes in a dinoflagellate *Alexandrium fundyense* in natural bloom condition relative to laboratory culture condition (56). Higher abundance and enzyme activity of intercellular CA protein from a dinoflagellate *Protoceratium reticulatum* is detected to sustain normal photosynthetic rates at low CO_2 condition (21). All these results indicated the vital role of CAs to adapt to low CO_2 condition during the blooming phases of *H. akashiwo* and *P. donghaiense*. Strikingly, cell membrane protein of solute carrier family 4, member 10 (SLC4A10) from *H. akashiwo*, responsible for transmembrane bicarbonate transport, was detected in the NB and BHA samples. Substantial contribution of SLC4 to CCMs under low CO_2 condition has been documented in diatoms (57, 58). In phytoplankton blooming phases, the rapid consumption of CO_2 and high alkaline carbonate

chemistry of seawater generated by high biomass leads to severe CO_2 limitation (59). Therefore, *H. akashiwo* cells expressed efficient HCO_3^- transport system and highly abundant CA to acquire sufficient CO_2 for carbon fixation during the bloom period.

The slow carboxylation reaction of RuBisCO is a critical rate-limiting step for carbon fixation and cell growth. Apart from the elevation of cellular CO_2 concentration, increased RuBisCO abundance represents another vital adaptive strategy to enhance the CO_2 fixation efficiency in phytoplankton (52). Higher proportion of RuBisCO from *H. akashiwo* was observed in comparison with that from *P. donghaiense* during the bloom periods (Fig. 5C). Among six distinct phytoplankton taxa, dinoflagellates exhibit the lowest substrate specificity factor for RuBisCO (50). The poor kinetics of RuBisCO and the consequential low photosynthetic efficiency have been proposed to be responsible for the slow growth rate of dinoflagellates (49). Combined with enzyme kinetics studies, higher abundance of RuBisCO from *H. akashiwo* reflected its higher carbon fixation efficiency than that from *P. donghaiense* during their bloom periods. *H. akashiwo* cells are also characterized by the presence of a great number of chloroplasts where carbon fixation occurs (60), consistent with our finding that *H. akashiwo* possessed high abundances of CA and RuBisCO. Taken together, the inorganic carbon transportation and fixation capabilities of *H. akashiwo* were more powerful than those of *P. donghaiense*, likely providing a genetic advantage that explains the earlier onset of *H. akashiwo* bloom.

Phosphorus uptake and metabolism. Nutrient availability determines cell growth rates and partially influences the niche partition of phytoplankton in marine environment (61, 62). Phosphorus (P) is a limiting nutrient for growth and productivity of phytoplankton in the ocean (63). Phytoplankton cells are known to be capable of balancing P uptake, metabolism and storage to maintain the bioavailability of inorganic phosphate (Pi) and dissolved organic phosphorus (DOP). As documented, *H. akashiwo* is less tolerant of P limitation than *P. minimum*, and low concentrations of ambient Pi eventually leads to the dissipation of *H. akashiwo* bloom (54). In the present study, the dissolved inorganic N/P ratio varied between 21.72 and 822.89 (higher than the Redfield ratio of 16:1), indicating that Pi limitation occurred during the bloom periods. At the end of *H. akashiwo*

bloom, the concentration of Pi was 0.03 μM. Whereas, the concentration of Pi was relatively high during bloom period of *P. donghaiense*, ranging from 0.11 μM to 0.21 μM. Thus, it is postulated that low concentration of ambient Pi was a crucial factor responsible for the dissipation of *H. akashiwo* bloom.

Solute carrier family 37 (glycerol-3-phosphate transporter), member 3 (SLC37A3) from *H. akashiwo* was detected in the BHA and BPD samples, while only low affinity inorganic phosphate transporter (PHO84) from *P. donghaiense* was detected in the three samples (Fig. 6A). SLC37A3, also known as sugar phosphate exchanger 3, is a sugar-phosphate antiporter that transports phosphate into the cell (64). In addition, vacuolar transporter chaperone 4 (VTC4), which is involved in metabolism of polyphosphate, was detected only from *H. akashiwo* in the HBA sample (Fig. 6A). Polyphosphate serves as both a major cellular phosphate reservoir and an energy storage pool that can be used as a source of ATP (65). Some phytoplankton species can acquire Pi to synthesize polyphosphate under Pi-sufficient conditions, and degrade polyphosphate to release Pi through up-regulation of VTC4 under Pi-deficient condition (66, 67). These results indicated that *H. akashiwo* initiates external phosphate transport and internal storage systems to adapt to low-Pi environments, thus supporting its bloom prior to that of *P. donghaiense*.

DOP serves as an important P source for phytoplankton under low-Pi conditions, but most DOPs must be converted to Pi by cell surface alkaline phosphatases (APs) before use (63, 64). An alkaline phosphatase D (phoD) belonging to the AP family was detected from *H. akashiwo* in the NB and BHA samples (Fig. 6A), indicating that the cells utilized extracellular DOPs under the low-Pi environment. However, we did not identify AP from *P. donghaiense* despite existence of its sequences in the database, suggesting that AP might be present at low abundance or was not expressed. Interestingly, 5'-nucleotidase from *P. donghaiense* was detected in the NB and BPD samples (Fig. 6A). Recently, 5'-nucleotidase is reported to take function at extracellular ATP hydrolysis to maintain growth in dinoflagellate *Karenia mikimotoi* (68). Similarly, the *in situ P. donghaiense* cells might rely on 5'-nucleotidase rather than AP to utilize extracellular ATP as P source during the bloom period. Utilization of the intracellular DOPs represents another important

297 adaptive strategy to manage low-Pi stress. For *H. akashiwo*, protein phosphatase in the BHA sample,
298 phospholipase in the NB and BHA samples, phosphatidylinositol phospholipase C and
299 3'(2'),5'-bisphosphate nucleotidase in the three samples were detected, while for *P. donghaiense*, acid
300 phosphatase in the BPD sample, protein phosphatase and phosphatase 2C in the three samples were
301 identified (Fig. 6A). Protein phosphatase, acid phosphatase and 3'(2'),5'-bisphosphate nucleotidase
302 hydrolyze phosphoric esters, while phospholipase and phosphatidylinositol phospholipase C
303 hydrolyze structural phospholipids to release phosphate (69-71). These enzymes and their homologs
304 involved in DOP reutilization are found to be highly expressed under P-deficient conditions (66-68).
305 The multiple but varied DOP utilization strategies enable *H. akashiwo* and *P. donghaiense* to adapt
306 to low-Pi concentration during their blooming periods.

307 **Nitrogen uptake and metabolism.** Nitrogen is an essential nutrient for phytoplankton growth. In
308 our study, concentrations of nitrogen decreased sharply during the bloom processes from *H.*
309 *akashiwo* to *P. donghaiense*. Ammonium transporter and nitrite transporter Nar1 from *H. akashiwo*
310 were detected in the three samples, while no inorganic nitrogen transporter from *P. donghaiense* was
311 detected (Fig. 6B). Compared with *P. donghaiense*, higher abundances of substrate-specific
312 transporters in *H. akashiwo* indicated stronger competitive ability for ammonium and nitrite of *H.*
313 *akashiwo*. A previous field study also reveals that the bloom of *H. akashiwo* occurs after the increase
314 of Pi and dissolved inorganic nitrogen concentrations while addition of phosphate and nitrate
315 promotes its earlier bloom (72).

316 Interestingly, polar amino acid transport system ATP-binding protein (ABC.PA.A) and
317 substrate-binding protein (ABC.PA.S) from *P. donghaiense* were identified in the three samples (Fig.
318 6B, Table S2). Although we did not measure the concentrations of amino acids, a significant
319 decrease of dissolved amino acids coupled with the spring bloom succession from diatom *S.*
320 *costatum* to *P. donghaiense* is observed in the same investigation area (22). Increasing evidences
321 suggest that certain dinoflagellate species prefer dissolved organic nutrients to inorganic nutrients
322 (73, 74). Taken together, after the dissipation of *H. akashiwo* bloom, *P. donghaiense* activated the
323 amino acid uptake system to maintain cell growth in an environment of low-inorganic and

high-organic nitrogen contents. Moreover, strong capability of amino acid acquisition promotes its bloom formation and maintenance in the presence of other co-existing phytoplankton species.

In marine phytoplankton, nitrate reductase (NR) and nitrite reductase (NiR) catalyze the reduction of NO_3^- to NH_4^+. The cellular reduced and extracellular imported NH_4^+ is assimilated into glutamate through the GS-GOGAT pathway, which is catalyzed by glutamine synthetase (GS) and glutamate synthase (GOGAT) (75). The ornithine-urea cycle (OUC) converts NH_4^+ into amino acids and links the amino acids metabolism, TCA cycle and GS-GOGAT pathway (76, 77). All these intracellular nitrogen metabolizing enzymes and some OUC enzymes were detected from *H. akashiwo* and *P. donghaiense* in the three samples. Meanwhile, higher proportions of GS, GOGAT, four OUC enzymes (argininosuccinate synthase, argininosuccinate lyase, carbamoyl-phosphate synthase and ornithine carbamoyltransferase) and lower proportions of NR and NiR from *H. akashiwo* in the NB and BHA samples were detected, compared with that from *P. donghaiense* in the NB and BPD samples (Fig. 6B). As the GS-GOGAT and OUC pathways catalyze incorporation of NH_4^+ into organic molecules, the higher expression of related proteins further validated the significant contribution of ambient ammonium to the bloom formation of *H. akashiwo*. As documented, *H. akashiwo* prefers to acquire ammonium under both nitrogen sufficient and sub-sufficient conditions (78). It is predictable that *H. akashiwo* had strong capability of utilizing various ambient sources of inorganic nitrogen, such as ammonium, nitrite and nitrate, whereas *P. donghaiense* relied on nitrate/nitrite and amino acids as nitrogen resources. The different nutritional niches of nitrogen resources partially facilitated the subsequent bloom occurrence from *H. akashiwo* to *P. donghaiense* in the coastal ECS.

Hydrolysis of organic matters. Lysosomes are spherical vesicles that contain hydrolytic enzymes for the breakdown of various biomolecules from extracellular environments and cellular obsolete components (79). Functions of lysosomes are well-studied in animals, and lysosome-like vacuoles have been found in some plants and phytoplankton species (80, 81). Higher proportions of lysosome-like proteins from *P. donghaiense* were detected than that from *H. akashiwo* in the three samples (Fig. 2B and 6C, Table S3). Several subunits of cathepsin and tripeptidyl-peptidase involved

in polypeptide hydrolysis were detected in both species (82). Beta-glucuronidase from *P. donghaiense*, catalyzing the hydrolysis of complex carbohydrates (83), was detected in the three samples. In addition, extracellular sulfatase Sulf, arylsulfatase subunit B, iduronate 2-sulfatase and N-acetylglucosamine-6-sulfatase from *P. donghaiense* were detected in the three samples. All these proteins catalyze the hydrolytic breakdown of complex sulfuric esters to release sulfate (84, 85). It has been reported that the dissolved organic carbon and nitrogen accumulate substantially during the bloom period of *H. akashiwo* and peak at the post-bloom stage (86). The utilization of dissolved organic matter by mixotrophic species, for example, *P. donghaiense*, proves advantageous for their geographical distribution of HABs (87, 88). *H. akashiwo* released a large amount of dissolved organic matters into seawaters at the dissipation stage, thus providing carbon, nitrogen, phosphorus and other nutrient sources for the cell growth and proliferation of *P. donghaiense*. Meanwhile, the high expression levels of various hydrolases utilizing organic matters in *P. donghaiense* supported this postulation to a certain degree.

Database construction for protein identification. For metaproteomic study, a suitable protein searching database is critical for achieving accurate functional and taxonomic characterization. Two main approaches have been developed to construct protein searching database: combining the public sequence data or conducting simultaneous metagenomic analysis (89, 90). Growing evidences suggest that protein sequences from the public database relative to the simultaneous metagenome will cause statistical bias on protein identification and then lead to different biological conclusions (90, 91). Sequencing simultaneous metagenome or metatransciptome, is therefore an ideal choice for metaproteomic study. When metagenome and/or metatransciptome are not available, constructing the most suitable database to reflect the real environmental community structure is an alternative choice. In our study, we constructed a database consisting of phytoplankton sequences from two public databases, transcriptome of bloom-causing species and *in situ* metatranscriptome (Table S4) to compensate for the lack of metagenome. Even though the database had only 5.7% of the protein sequences attributed to Ochrophyta (of which *H. akashiwo* belongs to), Ochrophyta proteins accounted for 24.6%, 33.5% and 17.8% of the total proteins in the NB, BHA and BPD samples.

Moreover, a high degree of similarity of taxonomic composition inferred from the protein and 18S rDNA gene data were also observed in the three samples. These results indicated that the combined database largely contained the potential species in the investigation area and it was suitable to unveil metabolic activities of each phytoplankton species during the bloom period, especially the two bloom-causing species.

CONCLUSION

Our metaproteomic study revealed different molecular behaviors of two co-existing phytoplankton species *H. akashiwo* and *P. donghaiense* during their bloom periods. *H. akashiwo* exhibited strong capabilities of light-harvesting, as well as acquisition and metabolism of inorganic carbon, nitrogen and phosphorus, thus facilitating its earlier bloom under the conditions of high turbidity and inorganic nutrient concentrations. In the blooming phase, *H. akashiwo* cells highly expressed low affinity phosphate transporter and activated intra- and extracellular organic phosphorus utilization to adapt to low-Pi stress. However, the low concentration of ambient Pi eventually led to the termination of *H. akashiwo* bloom. Whereas, *P. donghaiense* cells exhibited strong capabilities of acquisition and hydrolytic breakdown of extra- and intracellular organic matter in its blooming phase. Therefore, the different light-harvesting capability and nutritional niche divergence of the two co-existing phytoplankton species might drive the bloom occurrence under different ambient conditions. Our study sheds light on the molecular mechanisms of different phytoplankton blooms. Future efforts should be devoted to the metaproteomic studies of blooms involving different phytoplankton species, and the results will help us more comprehensively understand the formation mechanisms of phytoplankton blooms in the ocean.

MATERIALS AND METHODS

Field survey and sampling. Field investigation of the spring phytoplankton bloom in the coastal ECS was conducted through daily surveying of each station along the Za and Zb transects from May 1 to 21, 2014 (Fig. 1). During the investigation, the physical oceanographic parameters were

405 monitored by an onboard CTD. At each sampling station, three 50 mL surface seawater samples (1
406 m) were collected and fixed with Lugol's solution for microscopic examination. To avoid diel
407 interference, all samples for Chl *a*, 18S rDNA and metaproteomic analysis were collected with the
408 same procedure between 11:00 to 14:00 each day. The surface seawater samples (1 m) were first
409 filtered through a 200 μm nylon net, and then through a 1.6 μm GF/A membrane (Whatman™, GE
410 Healthcare Life science). Three 200 mL surface seawater samples at each sampling station were
411 collected for Chl *a* and nutrient measurements. The filtration membranes were kept at -20°C for Chl
412 *a* analysis and the filtrates were kept frozen for nutrient analysis. Two 1 L surface seawater samples
413 at each sampling station were collected and the filtration membranes were stored at -20 °C for 18S
414 rDNA analysis. For metaproteomic analysis, two 30-60 L surface seawater samples were collected
415 and the filtrates were frozen in liquid nitrogen immediately and then transferred for storage at
416 -80 °C.

417 **Chl *a* and nutrient measurements.** Chl *a* was extracted with 90% acetone, and then analyzed
418 using an Anglient series 1100 HPLC system fitted with a 3.5 μm Eclipse XDB C8 column (100×4.6
419 nm, Agilent Technolgies) with a modified procedure (92). Nutrients were analysed photometrically
420 using an autoanalyzer (model: SkalarSANplus). The analytical precision of NO_3^-, NH_4^+ and PO_4^{3-}
421 were 0.1 μM, 0.1 μM, and 0.05 μM, respectively.

422 **DNA extraction and 18S rDNA sequencing.** Before DNA extraction, the filtration membrane
423 was suspended in DNA lysis buffer (10 mM Tris pH 8.0; 100 mM EDTA pH 8.0; 0.5% SDS; 100
424 μg/mL proteinase K) and incubated at 55 °C for 2 days. Then, for each sample, DNAs with two
425 biological replicates were extracted following a previous protocol (93). The V4-V5 hypervariable
426 region of eukaryotic 18S rDNA was amplified with 528F and 706R primers (94). PCR amplification
427 was carried out in 30 μL reactions with 15 μL of Phusion® High-Fidelity PCR Master Mix (New
428 England Biolabs), 0.2 μM of forward and reverse primers and about 10 ng of template DNA.
429 Thermal cycling consisted of initial denaturation at 98 °C for 1 min, followed by 30 cycles of
430 denaturation at 98°C for 10 s, annealing at 50 °C for 30 s and elongation at 72°C for 60 s. The final
431 elongation was allowed to proceed at 72 °C for 5 min. A negative PCR control without template

DNA was included. All amplicons were then sequenced on a single run using the IlluminaMiSeq platform (2 x 250 bp). Paired-end reads from the original DNA fragments were merged using FLASH (95) and then assigned to each sample according to the unique barcodes. Sequences analysis was performed with the UPARSE software package (96) using the UPARSE-OTU and UPARSE-OTUref algorithms. Sequences with ≥ 97% similarity were assigned to the same operational taxonomic units (OTUs). Representative sequences were picked for each OTU using the RDP classifier (97) to annotate taxonomic information for each representative sequence against Silva release 119 (98).

Protein extraction, separation and LC-ESI-MS analysis. Proteins from two biological replicates of each sampling site were extracted following a modified protocol (33). Briefly, the filtration membrane with 10 mL Trizol reagent was sonicated in ice for 5 min. Subsequently, added 2 mL chloroform to the cell lysate, and held at room temperature for 5 min after being vortexed for 15 s, centrifuged at 12000 g for 15 min at 4 ºC, removed the top pale-yellow or colorless layer, and added 3 mL ethanol to resuspend the reddish bottom layer. The mixture was vortexed and centrifuged at 2000 g for 5 min at 4ºC, and then the supernatant was transferred to a new tube and added 10 mL isopropanol. The mixture was stored at -20ºC for at least 2 h for protein precipitation, then centrifuged at 14000 g for 30 min at 4ºC. After washing with 5 mL of 95% ethanol, the pellet obtained was dissolved in 0.5 M TEAB (Applied Biosystems, Milan, Italy). After centrifuging at 30 000g at 4 °C, an aliquot of the supernatant was taken for further analysis. Protein quantification was performed using a 2D Quant kit (GE Healthcare, San Francisco, CA).

After adjusting the pH to 8.5 with 1 M ammonium bicarbonate, total protein (100μg) from each sample was reduced with DTT for 1 h at 60 °C and carboxyamidomethylated with iodoacetamide for 45 min at room temperature in the dark. Each sample was digested twice using Trypsin Gold (Promega, Madison, WI, USA) with a ratio of protein:trypsin = 30:1 at 37 °C for 16 h. After desalting on a Strata-X C18 solid phase extraction column (Phenomenex), the trypsin-digested samples were evaporated and reconstituted in 0.5 M TEAB. Fractionation of peptide samples was performed by SCX chromatography using a LC-20AB HPLC pump system (Shimadzu, Kyoto,

459 Japan). The pre-dried peptide samples were re-dissolved in 4 mL buffer (25 mM NaH_2PO_4 in 25%
460 acetonitrile, pH 2.7) and loaded onto a 4.6 × 250 mm Ultremex SCX column containing 5 μg
461 particles (Phenomenex). The eluted peptides were separated into 20 fractions, desalted with a
462 Strata-X C18 column (Phenomenex) and vacuum-dried. Each fraction was re-dissolved in buffer A
463 (5% acetonitrile, 0.1% formic acid) and injected into a 2 cm C18 trap column of LC-20AD
464 nanoHPLC (Shimadzu, Kyoto, Japan). Peptides were eluted from the trap column and separated on
465 an analytical C18 column (75μm × 100 mm) with a 35 min linear gradient at 300 μL min^{-1} from 2 to
466 35% buffer B (95% acetonitrile, 0.1% formic acid), followed by 5 min linear gradient to 60%, 2 min
467 linear gradient to 80% and maintenance at 80% for 4 min. Upon completion of the gradients, the
468 column was washed with 90% buffer B and re-equilibrated with buffer A. Mass spectra acquisition
469 was performed with a Triple-TOF 5600 system (AB SCIEX, Concord, ON) fitted with a Nanospray
470 III source (AB SCIEX, Concord, ON) and a pulled quartz tip as the emitter (New Objectives,
471 Woburn, MA). Data were acquired using ion spray voltage of 2.5 kV, curtain gas of 30 psi, nebulizer
472 gas of 15 psi, and temperature of 150 ºC. For information dependent acquisition (IDA) scanning, the
473 mass range was from 350 to 1500 m/z, survey scans were acquired of 100 ms and the top 40 product
474 ion scans were collected with a threshold of 150 counts per second (counts/s) and with a 2+ to 5+
475 charge state of a total cycle time of 2.8 s. Four time bins were summed for each four-anode channel
476 scan at a pulse frequency value of 11 kHz and monitor frequency value of 40 GHz. Dynamic
477 exclusion was set for 1/2 of peak width (15 s), and then the precursor was refreshed off the exclusion
478 list.

479 **Protein identification and bioinformatics analysis.** Raw peptide data (.wiff) were converted to
480 the Mascot generic file format (.mgf) using the SCIEX MS Data Converter (version 1.3 beta). The
481 MS/MS peak lists were searched against the phytoplankton database, which was combined from four
482 sources (Table S4). Two of them were downloaded from the websites of National Center for
483 Biotechnology Information (NCBI) and Marine Microbial Eukaryote Transcriptome Sequencing
484 Project (MMETSP). The other two sequence databases included the transcriptomes of *P.*
485 *donghaiense* grown under the phosphorus-replete and -starved conditions, and the metatranscriptome

of non-bloom samples collected in the investigating area on Nov. 05, 2013 (4665287+245 (contaminant) sequences, 2.2 Gb). Protein identification and quantification were performed using the MetaPro-IQ approach (99). Briefly, a database search against the combined phytoplankton database was firstly performed to generate a reduced database that contains all possible proteins derived from peptide-spectrum matches (PSMs) for all samples using X!Tandem software (2017.2.1 version) without any criterions. The reduced database containing the resulting protein lists was then imported into MaxQuant software (1.6.1.0 version) for protein quantification (100). The following parameters were selected: trypsin specificity with allowance for one missed cleavages; fixed modifications of carbamidomethyl (C); variable modifications consisting of Gln->pyro-Glu (N-term Q), deamidation (N, Q) and oxidation (M); peptide charge, 2+, 3+ and 4+; 20 ppm of peptide mass tolerance; 0.05 Da of fragment mass tolerance; To reduce the probability of false peptide identification, the false discovery rate (FDR) was set to less than 1% at both PSM and protein levels. High-confidence proteins matching at least two peptides and one unique peptide were selected for further analysis.

Proteins identified by the same set or a subset of peptides were grouped together as one protein group. Leading proteins (defined as the top rank protein in a group; ranking is based on the number of peptide sequences, the number of PSMs and the sequence coverage) of the protein group were chosen out for further taxonomic and functional analysis (99). For taxonomic annotation, the matched sequences from NCBI, MMETSP and *P. donghaiense* transcriptome were species-specific and sequences from metatranscriptome were annotated against the NCBI non-redundant protein database (NCBInr) database for species assignment. For functional analysis, the matched protein sequences were annotated against the NCBInr and Kyoto Encyclopedia of Genes and Genomes (KEGG database. For proteome-based community structure analysis, relative abundances of each organismal group were calculated by summing their total protein abundances and then divided by the sum of all protein abundances in a sample (community-level analysis). For function comparisons, the relative abundance of each protein and metabolic KEGG pathway was calculated by summing the related protein abundances and then divided by the sum of all protein abundances in a species (species-level analysis).

The mass spectrometry proteomic data has been submitted to the ProteomeXchange Conssortium via the PRIDE partner repository with the data set identifier PXD014327.

ACKNOWLEDGEMENTS

This work was partially supported by research grants from the National Natural Science Foundation of China (Project No. 41425021 and 41606132) and the National Key Research Development Program of China (Project No. 2017YFC1404302) and D.Z. Wang was also supported by the 'Ten Thousand Talents Program' for leading talents in science and technological innovation.

We declare no competing interests.

REFERENCES

1. Sellner KG, Doucette GJ, Kirkpatrick GJ. 2003. Harmful algal blooms: causes, impacts and detection. J Ind Microbiol Bio 30:383–406.
2. Heisler J, Glibert P, Burkholder J, Anderson D, Cochlan W, Dennison W, Gobler C, Dortch Q, Heil C, Humphries E, Lewitus A, Magnien R, Marshall H, Sellner K, Stockwell D, Stoecker D, Suddleson M. 2008. Eutrophication and harmful algal blooms: a scientific consensus. Harmful Algae 8:3–13.
3. Gobler CJ, Lonsdale DJ, Boyer GL. 2005. A review of the causes, effects, and potential management of harmful brown tide blooms caused by *Aureococcus anophagefferens* (Hargraves et Sieburth). Estuaries 28:726–749.
4. Anderson DM, Alpermann TJ, Cembella AD, Collos Y, Masseret E, Montresor M. 2012. The globally distributed genus Alexandrium: multifaceted roles in marine ecosystems and impacts on human health. Harmful Algae 14:10–35.
5. Anderson DM, Cembella AD, Hallegraeff GM. 2012. Progress in understanding harmful algal blooms: paradigm shifts and new technologies for research, monitoring, and management. Ann Rev Mar Sci 4:143–176.
6. Hallegraeff GM. 2010. Ocean climate change, phytoplankton community responses, and harmful algal blooms: a formidable predictive challenge. J Phycol 46:220–235.
7. Zhou MJ, Shen ZL, Yu RC. 2008. Responses of a coastal phytoplankton community to increased nutrient input from the Changjiang (Yangtze) River. Con Shelf Res 28:1483–1489.
8. Anderson DM, Glibert PM, Burkholder JM. 2002. Harmful algal blooms and eutrophication: Nutrient sources,

composition, and consequences. Estuaries 25:704–726.

9. Gobler CJ, Doherty OM, Hattenrath-Lehmann TK, Griffith AW, Kang Y, Litaker RW. 2017. Ocean warming since 1982 has expanded the niche of toxic algal blooms in the North Atlantic and North Pacific oceans. Proc Natl Acad Sci USA 114:4975–4980.
10. O'Neil JM, Davis TW, Burford MA, Gobler CJ. 2012. The rise of harmful cyanobacteria blooms: The potential roles of eutrophication and climate change. Harmful Algae 14:313–334.
11. Xiao W, Liu X, Irwin AJ, Laws EA, Wang L, Chen B, Zeng Y, Huang B. 2018. Warming and eutrophication combine to restructure diatoms and dinoflagellates. Water Res 128:206–216.
12. Brand LE, Campbell L, Bresnan E. 2012. Karenia: The biology and ecology of a toxic genus. Harmful Algae 14:156–178.
13. Domingues RB, Barbosa A, Galvão H. 2005. Nutrients, light and phytoplankton succession in a temperate estuary (the Guadiana, south-western Iberia). Estuar Coas Shelf Sci 64:249–260.
14. Kremp A, Tamminen T, Spilling K. 2008. Dinoflagellate bloom formation in natural assemblages with diatoms: nutrient competition and growth strategies in Baltic spring phytoplankton. Aquat Microb Ecol 50:181–196.
15. Sunda WG, Hardison. 2010. Evolutionary tradeoffs among nutrient acquisition, cell size, and grazing defense in marine phytoplankton promote ecosystem stability. Mar Ecol Prog Ser 401:63–76.
16. Fan C, Glibert PM. 2005. Effects of light on nitrogen and carbon uptake during a *Prorocentrum minimum* bloom. Harmful Algae 4: 629-641.
17. Rost B, Riebesell U, Burkhardt S, Sültemeyer D. 2003. Carbon acquisition of bloom-forming marine phytoplankton. Limnol Oceanogr 48:55–67.
18. Tortell PD, DiTullio GR, Sigman DM, Morel FMM. 2002. CO_2 effects on taxonomic composition and nutrient utilization in an Equatorial Pacific phytoplankton assemblage. Mar Ecol Progs Ser 236:37–43.
19. Dyhrman ST, Anderson DM. 2003. Urease activity in cultures and field populations of the toxic dinoflagellate *Alexandrium*. Limnol Oceanogr 48:647-655.
20. Rost B, Richter KU, Riebesell ULF, Hansen PJR. 2006. Inorganic carbon acquisition in red tide dinoflagellates. Plant Cell Environ 29:810–822.
21. Ratti S, Giordano M, Morse D. 2007. CO_2-concentrating mechanisms of the potentially toxic dinoflagellate *Protoceratium reticulatum* (Dinophyceae, Gonyaulacales). J Phycol 43:693-701.
22. Zhang G, Liang S, Shi X, Han X. 2015. Dissolved organic nitrogen bioavailability indicated by amino acids during a diatom to dinoflagellate bloom succession in the Changjiang River estuary and its adjacent shelf.

574 Mar Chem 176:83–95.
575 23. Accoroni S, Totti C, Razza E, Congestri R, Campanelli A, Marini M, Ellwood NTW. 2017. Phosphatase
576 activities of a microepiphytic community during a bloom of *Ostreopsis* cf. *ovata* in the northern Adriatic Sea.
577 Water Res 120: 272-279.
578 24. Zhang Y, Lin X, Shi X, Lin L, Luo H, Li L, Lin S. 2019. Metatranscriptomic signatures associated with
579 phytoplankton regime shift from diatom dominance to a dinoflagellate bloom. Front Microbiol 10:590.
580 25. McLean TI. 2013. "Eco-omics": A review of the application of genomics, transcriptomics, and proteomics for
581 the study of the ecology of harmful algae. Microb Ecol 65:901–915.
582 26. Wang D, Zhang H, Zhang Y, Zhang S. 2014. Marine dinoflagellate proteomics: Current status and future
583 perspectives. J Proteomics 105:121–132.
584 27. Gobler CJ, Berry DL, Dyhrman ST, Wilhelm SW, Salamov A, Lobanov AV, Zhang Y, Collier JL, Wurch LL,
585 Kustka AB, Dill BD, Shah M, VerBerkmoes NC, Kuo A, Terry A, Pangilinan J, Lindquist EA, Lucas S,
586 Paulsen IT, Hattenrath-Lehmann TK, Talmage SC, Walker EA, Koch F, Burson AM, Marcoval MA, Tang YZ,
587 LeCleir GR, Coyne KJ, Berg GM, Bertrand EM, Saito MA, Gladyshev VN, Grigoriev IV. 2011. Niche of
588 harmful alga *Aureococcus anophagefferens* revealed through ecogenomics. Proc Natl Acad Sci USA
589 108:4352–4357.
590 28. Alexander H, Jenkins BD, Rynearson TA, Dyhrman ST. 2015. Metatranscriptome analyses indicate resource
591 partitioning between diatoms in the field. Proc Natl Acad Sci USA 112:E2182-90.
592 29. Alexander H, Rouco M, Haley ST, Wilson ST, Karl DM, Dyhrman ST. 2015. Functional group-specific traits
593 drive phytoplankton dynamics in the oligotrophic ocean. Proc Natl Acad Sci USA 112:E5972-5979.
594 30. Gong W, Browne J, Hall N, Schruth D, Paerl H, Marchetti A. 2016. Molecular insights into a dinoflagellate
595 bloom. ISME J 11:439-452.
596 31. Marchetti A, Schruth DM, Durkin CA, Parker MS, Kodner RB, Berthiaume CT, Morales R, Allen AE,
597 Armbrust EV. 2012. Comparative metatranscriptomics identifies molecular bases for the physiological
598 responses of phytoplankton to varying iron availability. Proc Natl Acad Sci USA 109:E317–E325.
599 32. Poulson-Ellestad KL, Jones CM, Roy J, Viant MR, Fernández FM, Kubanek J, Nunn BL. 2014.
600 Metabolomics and proteomics reveal impacts of chemically mediated competition on marine plankton. Proc
601 Natl Acad Sci USA 111:9009-9014.
602 33. Zhang H, Wang D, Xie Z, Zhang S, Wang M, Lin L. 2015. Comparative proteomics reveals highly and
603 differentially expressed proteins in field-collected and laboratory-cultured blooming cells of the diatom
604 *Skeletonema costatum*. Environ Microbiol 17:3976–3991.

34. Tse SPK, Lo SCL. 2017. Comparative proteomic studies of a *Scrippsiella acuminata* bloom with its laboratory-grown culture using a ^{15}N-metabolic labeling approach. Harmful Algae 67: 26-35.

35. He X, Bai Y, Pan D, Chen CAT, Cheng Q, Wang D, Gong F. 2013. Satellite views of the seasonal and interannual variability of phytoplankton blooms in the eastern China seas over the past 14 yr (1998-2011). Biogeosciences 10:4721–4739.

36. Zhou Z, Yu R, Zhou M. 2017. Seasonal succession of microalgal blooms from diatoms to dinoflagellates in the East China Sea: A numerical simulation study. Ecol Model 360:150–162.

37. Ji N, Lin L, Li L, Yu L, Zhang Y, Luo H, Li M, Shi X, Wang D, Lin S. 2018. Metatranscriptome analysis reveals environmental and diel regulation of a *Heterosigma akashiwo* (raphidophyceae) bloom. Environ Microbiol 20:1078–1094.

38. Spilling K, Olli K, Lehtoranta J, Kremp A, Tedesco L, Tamelander T, Klais R, Peltonen H, Tamminen T. 2018. Shifting diatom-dinoflagellate dominance during spring bloom in the Baltic sea and its potential effects on biogeochemical cycling. Front Mar Sci 5:327.

39. Irwin AJ, Nelles AM, Finkel ZV. 2012. Phytoplankton niches estimated from field data. Limnol Oceanogr 57:787-797.

40. Kempton J, Keppler CJ, Lewitus A, Shuler A, Wilde S. 2008. A novel *Heterosigma akashiwo* (Raphidophyceae) bloom extending from a South Carolina bay to offshore waters. Harmful Algae 7:235–240.

41. Livingston RJ. 2007. Phytoplankton bloom effects on a gulf estuary: water quality changes and biological response. Ecol Appl 17:110-128.

42. Green BR, Durnford DG. 1996. The chlorophyll-carotenoid proteins of oxygenic photosynthesis. Annu Rev Plant Physiol Plant Mol Biol 47:685–714.

43. Hu Z, R Mulholland M, Xu N, Duan S. 2016. Effects of temperature, irradiance and pCO_2 on the growth and nitrogen utilization of Prorocentrum donghaiense. Aquat Microb Ecol 77:155–166.

44. Zhang Y, Fu FX, Whereat E, Coyne KJ, Hutchins DA. 2006. Bottom-up controls on a mixed-species HAB assemblage: A comparison of sympatric *Chattonella subsalsa* and *Heterosigma akashiwo* (Raphidophyceae) isolates from the Delaware Inland Bays, USA. Harmful Algae 5:310–320.

45. Satoh E, Watanabe MM, Fujii T. 1987. Photoperiodic regulation of cell division and chloroplast replication in Heterosigma akashiwo. Plant Cell Physiol 28:1093–1099.

46. Gallegos CL, Bergstrom PW. 2005. Effects of a *Prorocentrum minimum* bloom on light availability for and potential impacts on submersed aquatic vegetation in upper Chesapeake Bay. Harmful Algae 4:553-574.

47. Collier JL, Grossman AR. 1994. A small polypeptide triggers complete degradation of light-harvesting

phycobiliproteins in nutrient-deprived cyanobacteria. EMBO J 13:1039-1047.

48. Kiyota H, Hirai MY, Ikeuchi M. 2014. NblA1/A2-dependent homeostasis of amino acid pools during nitrogen starvation in *Synechocystis* sp. PCC 6803. Metabolites 4:517-531.

49. Tortell PD. 2000. Evolutionary and ecological perspectives on carbon acquisition in phytoplankton. Limnol Oceanogr 45:744–750.

50. Badger MR, Andrews TJ, Whitney SM, Ludwig M, Yellowlees DC, Leggat W, Price GD. 1998. The diversity and coevolution of Rubisco, plastids, pyrenoids, and chloroplast-based CO_2-concentrating mechanisms in algae. Cana J Bot 76:1052–1071.

51. Hartman FC, Harpel MR. 1994. Structure, function, regulation, and assembly of D-ribulose-1,5-bisphosphate carboxylase/oxygenase. Annu Rev Biochem 63:197–234.

52. Reinfelder JR. 2011. Carbon concentrating mechanisms in eukaryotic marine phytoplankton. Ann Rev Mar Sci 3:291–315.

53. Henry RP. 1996. Multiple roles of carbonic anhydrase in cellular transport and metabolism. Annu Rev Physiol 58:523–538.

54. Fu FX, Zhang Y, Warner ME, Feng Y, Sun J, Hutchins DA. 2008. A comparison of future increased CO_2 and temperature effects on sympatric *Heterosigma akashiwo* and *Prorocentrum minimum*. Harmful Algae 7:76–90.

55. Nimer NA, Iglesias-Rodriguez MD, Merrett MJ. 1997. Bicarbonate utilization by marine phytoplankton species. J Phycol 33:625–631.

56. Zhuang Y, Zhang H, Hannick L, Lin S. 2015. Metatranscriptome profiling reveals versatile N-nutrient utilization, CO_2 limitation, oxidative stress, and active toxin production in an *Alexandrium fundyense* bloom. Harmful Algae 67: 60-70.

57. Nakajima K, Tanaka A, Matsuda Y. 2013. SLC4 family transporters in a marine diatom directly pump bicarbonate from seawater. Proc Natl Acad Sci USA 110:1767–1772.

58. Perland E, Fredriksson R. 2017. Classification systems of secondary active transporters. Trends Pharmacol Sci 38:305–315.

59. Kranz SA, Young JN, Hopkinson BM, Goldman JAL, Tortell PD, Morel FMM. 2015. Low temperature reduces the energetic requirement for the CO_2 concentrating mechanism in diatoms. New Phytol 205:192–201.

60. Hara Y, Chihara M. 1987. Morphology, ultrastructure and taxonomy of the raphidophycean alga *Heterosigma akashiwo*. J Plant Res 100:151–163.

667 61. Irwin AJ, Finkel ZV, Müller-Karger FE, Troccoli Ghinaglia L. 2015. Phytoplankton adapt to changing ocean
668 environments. Proc Natl Acad Sci USA 112:5762–5766.
669 62. Moore CM, Mills MM, Arrigo KR, Berman-Frank I, Bopp L, Boyd PW, Galbraith ED, Geider RJ, Guieu C,
670 Jaccard SL, Jickells TD, La Roche J, Lenton TM, Mahowald NM, Marañón E, Marinov I, Moore JK,
671 Nakatsuka T, Oschlies A, Saito MA, Thingstad TF, Tsuda A, Ulloa O. 2013. Processes and patterns of oceanic
672 nutrient limitation. Nat Geosci 6:701-710.
673 63. Falkowski PG, Raven JA. 2007. Aquatic Photosynthesis. (Second Edition), STU - Student edition. Princeton
674 University Press.
675 64. Lin S, Litaker RW, Sunda WG. 2016. Phosphorus physiological ecology and molecular mechanisms in marine
676 phytoplankton. J Phycol 52:10–36.
677 65. Kornberg A, Rao NN, Ault-Riché, D. 1999. Inorganic polyphosphate: a molecule of many functions. Annu
678 Rev Biochem 68:89–125.
679 66. Dyhrman ST, Jenkins BD, Rynearson TA, Saito MA, Mercier ML, Alexander H, Whitney LP, Drzewianowski
680 A, Bulygin VV, Bertrand EM, Wu Z, Benitez-Nelson C, Heithoff A. 2012. The transcriptome and proteome of
681 the diatom *Thalassiosira pseudonana* reveal a diverse phosphorus stress response. PLoS ONE 7:e33768.
682 67. Zhang SF, Yuan CJ, Chen Y, Chen XH, Li DX, Liu JL, Lin L, Wang D. 2016. Comparative transcriptomic
683 analysis reveals novel insights into the adaptive response of *Skeletonema costatum* to changing ambient
684 phosphorus. Front Microbiol 7:1476.
685 68. Luo H, Lin X, Li L, Lin L, Zhang C, Lin S. 2017. Transcriptomic and physiological analyses of the
686 dinoflagellate *Karenia mikimotoi* reveal non-alkaline phosphatase-based molecular machinery of ATP
687 utilisation. Environ Microbiol 19:4506–4518.
688 69. Park HJ, Choi YD, Song SI, Kwon HB, Oh NI, Cheong JJ. 2013. Overexpression of the 3′(2′),5′-bisphosphate
689 nucleotidase gene AtAHL confers enhanced resistance to *Pectobacterium carotovorum* in Arabidopsis. J
690 Korean Soc Appl Biol Chem 56:21–26.
691 70. Pleskot R, Li J, Žárský V, Potocký M, Staiger CJ. 2013. Regulation of cytoskeletal dynamics by
692 phospholipase D and phosphatidic acid. Trends Plant Sci 18:496–504.
693 71. Shi X, Lin X, Li L, Li M, Palenik B, Lin S. 2017. Transcriptomic and microRNAomic profiling reveals
694 multi-faceted mechanisms to cope with phosphate stress in a dinoflagellate. ISME J 11:2209–2218.
695 72. Shikata T, Yoshikawa S, Matsubara T, Tanoue W, Yamasaki Y, Shimasaki Y, Matsuyama Y, Oshima Y,
696 Jenkinson IR, Honjo T. 2008. Growth dynamics of *Heterosigma akashiwo* (Raphidophyceae) in Hakata Bay,
697 Japan. Eur J Phycol 43:395–411.

73. Altman JC, Paerl HW. 2012. Composition of inorganic and organic nutrient sources influences phytoplankton community structure in the New River Estuary, North Carolina. Aquat Ecol 46:269–282.

74. Dyhrman ST, Anderson DM. 2003. Urease activity in cultures and field populations of the toxic dinoflagellate *Alexandrium*. Limnol Oceanogr 48:647–655.

75. Takabayashi M, Wilkerson FP, Robertson D. 2005. Response of glutamine synthetase gene transcription and enzyme activity to external nitrogen sources in the diatom *Skeletonema costatum* (Bacillariophyceae). J Phycol 41:84–94.

76. Allen AE, Dupont CL, Oborník M, Horák A, Nunes-Nesi A, McCrow JP, Zheng H, Johnson DA, Hu H, Fernie AR, Bowler C. 2011. Evolution and metabolic significance of the urea cycle in photosynthetic diatoms. Nature 473:203–207.

77. Dagenais-Bellefeuille S, Morse D. 2013. Putting the N in dinoflagellates. Front Microbiol 4:369.

78. Herndon J, Cochlan WP. 2007. Nitrogen utilization by the raphidophyte *Heterosigma akashiwo*: Growth and uptake kinetics in laboratory cultures. Harmful Algae 6:260–270.

79. Settembre C, Fraldi A, Medina DL, Ballabio A. 2013. Signals from the lysosome: a control centre for cellular clearance and energy metabolism. Nat Rev Mol Cell Biol 14:283-296.

80. Arora M, Anil AC, Burgess K, Delany J, Mesbahi E. 2015. Asymmetric cell division and its role in cell fate determination in the green alga *Tetraselmis indica*. J Biosciences 40:921–927.

81. Li SC, Kane PM. 2009. The yeast lysosome-like vacuole: endpoint and crossroads. BBA 1793:650–663.

82. Domsalla A, Melzig MF. 2008. Occurrence and properties of proteases in plant latices. Planta Med 74:699–711.

83. Jain S, Drendel WB, Chen ZW, Mathews FS, Sly WS, Grubb JH. 1996. Structure of human β-glucuronidase reveals candidate lysosomal targeting and active-site motifs. Nat Struct Biol 3:375-381.

84. Huang Y, Mao Y, Buczek-Thomas JA, Nugent MA, Zaia J. 2014. Oligosaccharide substrate preferences of human extracellular sulfatase Sulf2 using liquid chromatography-mass spectrometry based glycomics approaches. PLoS ONE 9:e105143.

85. Roy AB. 1976. Sulphatases, lysosomes and disease. Aust J Exp Biol Med Sci 54:111–135.

86. Suksomjit M, Nagao S, Ichimi K, Yamada T, Tada K. 2009. Variation of dissolved organic matter and fluorescence characteristics before, during and after phytoplankton bloom. J Oceanogra 65:835–846.

87. Burkholder JM, Glibert PM, Skelton HM. 2008. Mixotrophy, a major mode of nutrition for harmful algal species in eutrophic waters. Harmful Algae 8:77–93.

88. Jeong HJ, Du Yoo Y, Kim JS, Seong KA, Kang NS, Kim TH. 2010. Growth, feeding and ecological roles of

729 the mixotrophic and heterotrophic dinoflagellates in marine planktonic food webs. Ocean Sci J 45:65–91.
730 89. Wang DZ, Xie ZX, Zhang SF. 2014. Marine metaproteomics: current status and future directions. J
731 Proteomics 97:27-35.
732 90. Timmins-Schiffman E, May DH, Mikan M, Riffle M, Frazar C, Harvey HR, Noble WS, Nunn BL. 2017.
733 Critical decisions in metaproteomics: achieving high confidence protein annotations in a sea of unknowns.
734 ISME J 11:309-314.
735 91. Riffle M, May DH, Timmins-Schiffman E, Mikan MP, Jaschob D, Noble WS, Nunn BL. 2018. MetaGOmics:
736 a web-based tool for peptide-centric functioanl and toxonomic analysis of metaproteomics data. Proteomes
737 6:2.
738 92. van Heukelem L, Thomas CS. 2001. Computer-assisted high-performance liquid chromatography method
739 development with applications to the isolation and analysis of phytoplankton pigments. J Chromatogr A
740 910:31–49.
741 93. Yuan J, Li M, Lin S. 2015. An improved DNA extraction method for efficient and quantitative recovery of
742 phytoplankton diversity in natural assemblages. PLoS ONE 10:e0133060.
743 94. Cheung MK, Au CH, Chu KH, Kwan HS, Wong CK. 2010. Composition and genetic diversity of
744 picoeukaryotes in subtropical coastal waters as revealed by 454 pyrosequencing. ISME J 4:1053–1059.
745 95. Magoč T, Salzberg SL. 2011. FLASH: fast length adjustment of short reads to improve genome assemblies.
746 Bioinformatics 27:2957–2963.
747 96. Edgar RC. 2013. UPARSE: highly accurate OTU sequences from microbial amplicon reads. Nat Methods
748 10:996–998.
749 97. Cole JR, Wang Q, Cardenas E, Fish J, Chai B, Farris RJ, Kulam-Syed-Mohideen AS, McGarrell DM, Marsh T,
750 Garrity GM, Tiedje JM. 2009. The Ribosomal Database Project: improved alignments and new tools for
751 rRNA analysis. Nucleic Acids Res 37:141-145.
752 98. Quast C, Pruesse E, Yilmaz P, Gerken J, Schweer T, Yarza P, Peplies J, Glöckner FO. 2013. The SILVA
753 ribosomal RNA gene database project: improved data processing and web-based tools. Nucleic Acids Res
754 41:590-596.
755 99. Zhang X, Ning Z, Mayne J, Moore JI, Li J, Butcher J, Deeke SA, Chen R, Chiang C, Wen M, Mack D, Stintzi
756 A, Figeys D. 2016. MetaPro-IQ: a universal metaproteomic approach to studying human and mouse gut
757 microbiota. Microbiome 4:31.
758 100. Cox J, Mann M. 2008. MaxQuant enables high peptide identification rates, individualized p.p.b.-range mass
759 accuracies and proteome-wide protein quantification. Nat Biotechnol 26:1367–1372.

760 **FIGURE LEGENDS**

761 **FIG 1** Sampling locations of the field investigation. Each spot from the Za and Zb transects
762 represents sampling station. The non-bloom (NB) and blooming *H. akashiwo* (BHA) samples were
763 collected at station Za3 (star) on May 2 and 7, and the blooming *P. donghaiense* (BPD) sample was
764 collected at station Zb7 (star) on May 21.

765 **FIG 2** Pysiochemical conditions during the investigaiton. (A) Bloom process of *H. akashiwo*
766 occurred at station Za3. (B) Bloom process of *P. donghaiense* occurred at station Zb7.

767 **FIG 3** Protein information and taxonomic compostition of the NB, BHA and BPD samples. (A)
768 Protein number of each phytoplankton group. (B) Percentage of each phytoplankton group based on
769 protein abundances. (C) Percentage of each phytoplankton group based on 18S rDNA gene
770 abundances.

771 **FIG 4** Heatmap of protein proportions at KEGG categories in the NB, BHA and BPD samples. (A)
772 Function classfication of *H. akashiwo* and *P. donghaiense* in the three samples. Color gradient
773 indicates the proportion of protein abundances mapped to each KEGG category of the total
774 KEGG-annotated protein abudances in one species of each sample. (B) Abundance ratio of *H.*
775 *akashiwo* to *P. donghaiense* at KEGG categories from each pair comparison. FC indicates fold
776 change of *H. akashiwo* to *P. donghaiense*. NB/NB represents comparison between *H. akashiwo* and
777 *P. donghaiense* in the NB sample, and BHA/BPD represents comparison between *H. akashiwo* in the
778 BHA sample and *P. donghaiense* in the BPD sample.

779 **FIG 5** Comparisons of protein abundances between the species of *H. akashiwo* and *P. donghaiense*
780 in the NB, BHA and BPD samples. (A) Light-harvesting proteins. (B) Inorganic carbon assimilation
781 proteins. (C) Carbon fixation proteins. CA: carbonic anhydrase; LHCA1: light-harvesting complex I
782 chlorophyll a/b binding protein 1; LHCA4: light-harvesting complex I chlorophyll a/b binding
783 protein 4; LHCB3: light-harvesting complex II chlorophyll a/b binding protein 3; LHCB5:
784 light-harvesting complex II chlorophyll a/b binding protein 5; RBCII: ribulose 1,5-bisphosphate
785 carboxylase oxygenase, form II; RBCL: ribulose 1,5-bisphosphate carboxylase oxygenase, large
786 subunit; RBCS: ribulose 1,5-bisphosphate carboxylase oxygenase, small subunit. SLC4A10: solute

carrier family 4 (sodium bicarbonate cotransporter), member 10.

FIG 6 Comparisons of protein abundances between the bloom species of *H. akashiwo* and *P. donghaiense* in the NB, BHA and BPD samples. (A) Phosphorus metabolism related proteins. (B) Nitrogen metabolism related proteins. (C) Hydrolytic enzymes. 5'-NT: 5'-nucleotidase; ABC.PA.A: polar amino acid transport system ATP-binding protein; ABC.PA.S: polar amino acid transport system substrate-binding protein; ACP: acid phosphatase; AMT: ammonium transporter; ARSA: arylsulfatase A; ARSB: arylsulfatase B; ARS I_J: arylsulfatase I_J; AsL: argininosuccinate lyase; AsuS: argininosuccinate synthase; BPNT1: 3'(2'),5'-bisphosphate nucleotidase; CPB: cysteine peptidase B; CPS: carbamoyl-phosphate synthase; CTS: cathepsin; GNS: N-acetylglucosamine-6-sulfatase; GOGAT1: glutamate synthase (NADPH/NADH); GOGAT2: glutamate synthase (ferredoxin); GS: glutamine synthetase; GUSB: beta-glucuronidase; IDS: iduronate 2-sulfatase; Nar1: nitrite transporter NirC; NiR: nitrite reductase; NR: nitrate reductase; OTC: ornithine carbamoyltransferase; PHO84: MFS transporter, PHS family, inorganic phosphate transporter; phoD: alkaline phosphatase D; PLCD: phosphatidylinositol phospholipase C; PLD: phospholipase; PP: protein phosphatase; PP2C: protein phosphatase 2C; SLC37A3: solute carrier family 37 (glycerol-3-phosphate transporter), member3; SULF: extracellular sulfatase Sulf; TPP1: tripeptidyl-peptidase I; TPP2: tripeptidyl-peptidase II; VTC4: vacuolar transporter chaperone 4.

FIG 7 Summary of the key molecular events occurring at the *H. akashiwo* and *P. donghaiense* cells during their bloom periods. (A) *H. akashiwo* of the NB sample. (B) *P. donghaiense* of the NB sample. (C) *H. akashiwo* of the BHA sample. (D) *P. donghaiense* of the BPD sample. The red and green colors represent higher and lower proportions of metabolic processes and enzymes of one species relative to the other species in the same blooming phase, and the gray color indicates no dection. The arrow represents the sample point. Protein abbreviations are annotated in FIG 5 and 6.

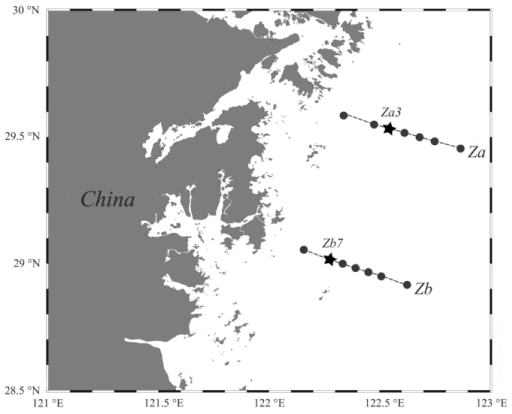

FIG 1 Sampling locations of the field investigation. Each spot from the Za and Zb transects represents sampling station. The non-bloom (NB) and blooming *H. akashiwo* (BHA) samples were collected at station Za3 (star) on May 2 and 7, and the blooming *P. donghaiense* (BPD) sample was collected at station Zb7 (star) on May 21.

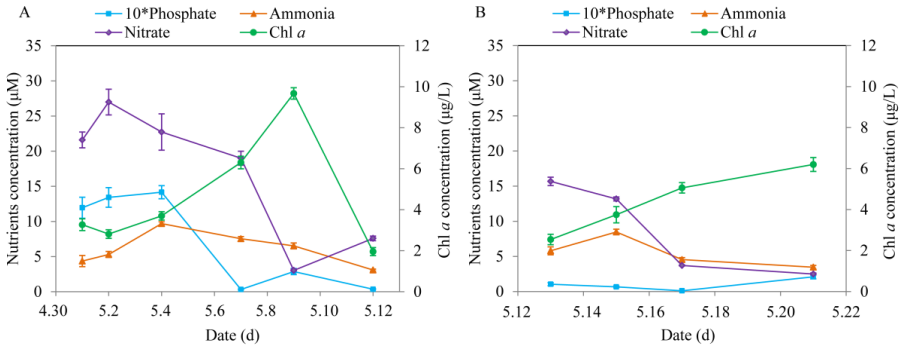

FIG 2 Pysiochemical conditions during the investigaiton. (A) Bloom process of *H. akashiwo* occurred at station Za3. (B) Bloom process of *P. donghaiense* occurred at station Zb7.

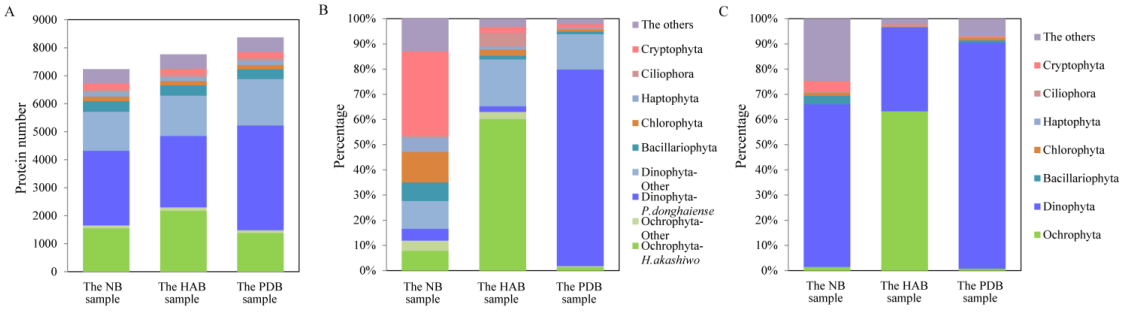

FIG 3 Protein information and taxonomic compostition of the NB, BHA and BPD samples. (A) Protein number of each phytoplankton group. (B) Percentage of each phytoplankton group based on protein abundances. (C) Percentage of each phytoplankton group based on 18S rDNA gene abundances.

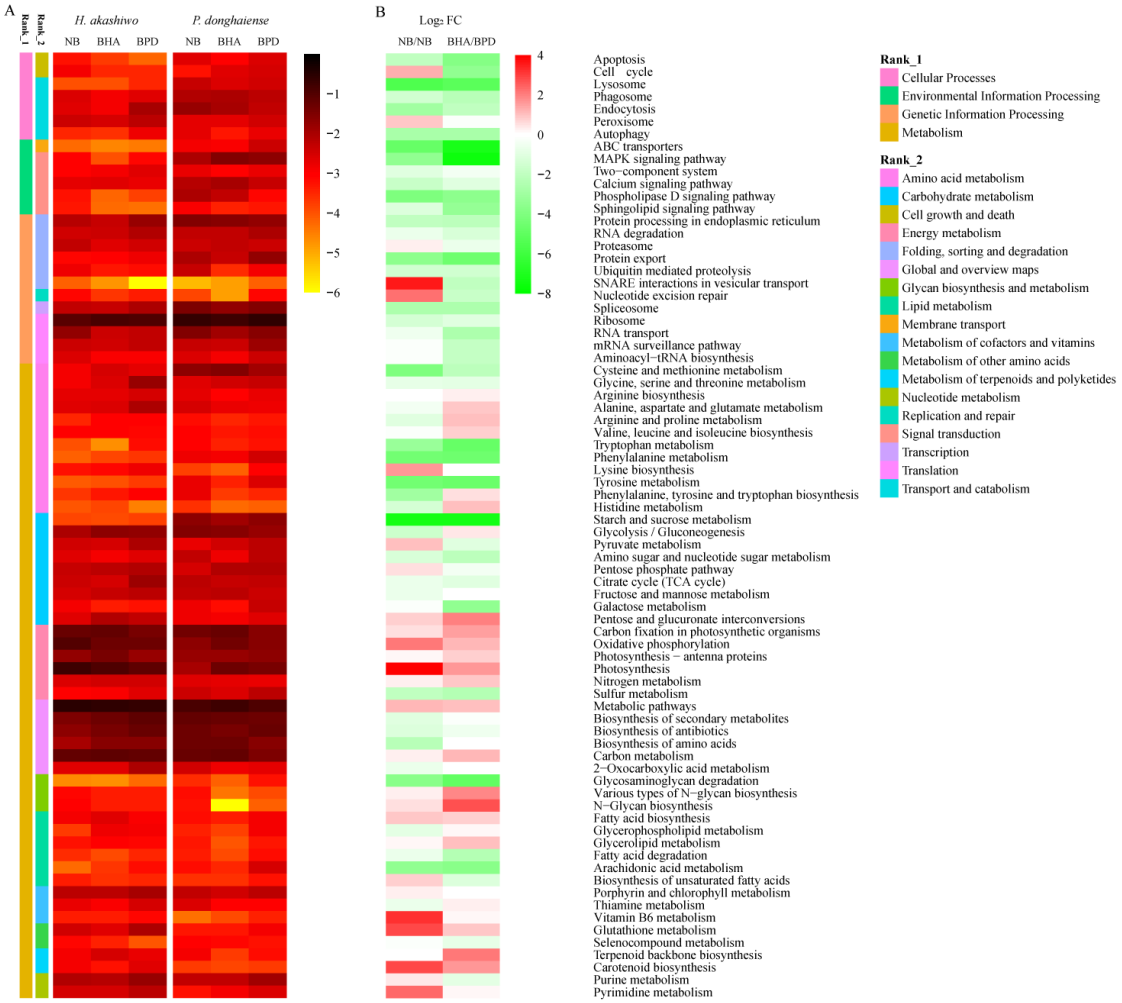

FIG 4 Heatmap of protein proportions at KEGG categories in the NB, BHA and BPD samples. (A) Function classfication of *H. akashiwo* and *P. donghaiense* in the three samples. Color gradient indicates the proportion of protein abundances mapped to each KEGG category of the total KEGG-annotated protein abudances in one species of each sample. (B) Abundance ratio of *H. akashiwo* to *P. donghaiense* at KEGG categories from each pair comparison. FC indicates fold change of *H. akashiwo* to *P. donghaiense*. NB/NB represents comparison between *H. akashiwo* and *P. donghaiense* in the NB sample, and BHA/BPD represents comparison between *H. akashiwo* in the BHA sample and *P. donghaiense* in the BPD sample.

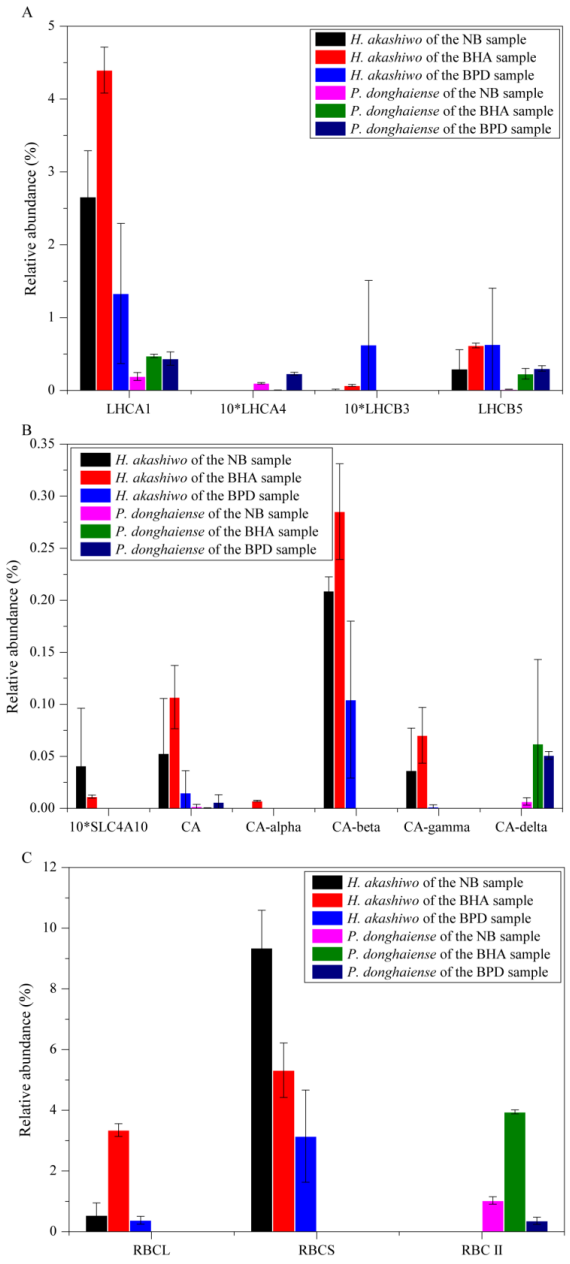

873

874 **FIG 5** Comparisons of protein abundances between the species of *H. akashiwo* and *P. donghaiense* in the NB,
875 BHA and BPD samples. (A) Light-harvesting proteins. (B) Inorganic carbon assimilation proteins. (C) Carbon
876 fixation proteins. CA: carbonic anhydrase; LHCA1: light-harvesting complex I chlorophyll a/b binding protein 1;
877 LHCA4: light-harvesting complex I chlorophyll a/b binding protein 4; LHCB3: light-harvesting complex II
878 chlorophyll a/b binding protein 3; LHCB5: light-harvesting complex II chlorophyll a/b binding protein 5; RBCII:
879 ribulose 1,5-bisphosphate carboxylase oxygenase, form II; RBCL: ribulose 1,5-bisphosphate carboxylase
880 oxygenase, large subunit; RBCS: ribulose 1,5-bisphosphate carboxylase oxygenase, small subunit. SLC4A10:
881 solute carrier family 4 (sodium bicarbonate cotransporter), member 10.

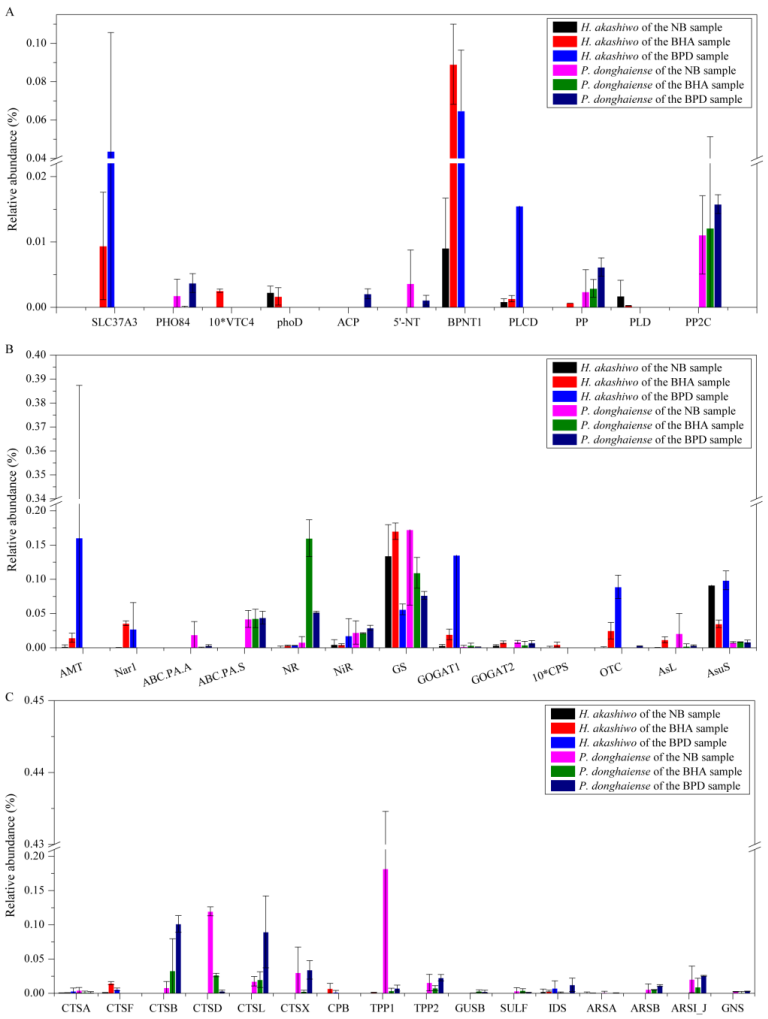

882

883 **FIG 6** Comparisons of protein abundances between the bloom species of *H. akashiwo* and *P. donghaiense* in the
884 NB, BHA and BPD samples. (A) Phosphorus metabolism related proteins. (B) Nitrogen metabolism related
885 proteins. (C) Hydrolytic enzymes. 5'-NT: 5'-nucleotidase; ABC.PA.A: polar amino acid transport system
886 ATP-binding protein; ABC.PA.S: polar amino acid transport system substrate-binding protein; ACP: acid
887 phosphatase; AMT: ammonium transporter; ARSA: arylsulfatase A; ARSB: arylsulfatase B; ARS I_J: arylsulfatase
888 I_J; AsL: argininosuccinate lyase; AsuS: argininosuccinate synthase; BPNT1: 3'(2'),5'-bisphosphate nucleotidase;
889 CPB: cysteine peptidase B; CPS: carbamoyl-phosphate synthase; CTS: cathepsin; GNS:
890 N-acetylglucosamine-6-sulfatase; GOGAT1: glutamate synthase (NADPH/NADH); GOGAT2: glutamate synthase
891 (ferredoxin); GS: glutamine synthetase; GUSB: beta-glucuronidase; IDS: iduronate 2-sulfatase; Nar1: nitrite
892 transporter NirC; NiR: nitrite reductase; NR: nitrate reductase; OTC: ornithine carbamoyltransferase; PHO84: MFS
893 transporter, PHS family, inorganic phosphate transporter; phoD: alkaline phosphatase D; PLCD:
894 phosphatidylinositol phospholipase C; PLD: phospholipase; PP: protein phosphatase; PP2C: protein phosphatase
895 2C; SLC37A3: solute carrier family 37 (glycerol-3-phosphate transporter), member3; SULF: extracellular sulfatase
896 Sulf; TPP1: tripeptidyl-peptidase I; TPP2: tripeptidyl-peptidase II; VTC4: vacuolar transporter chaperone 4.

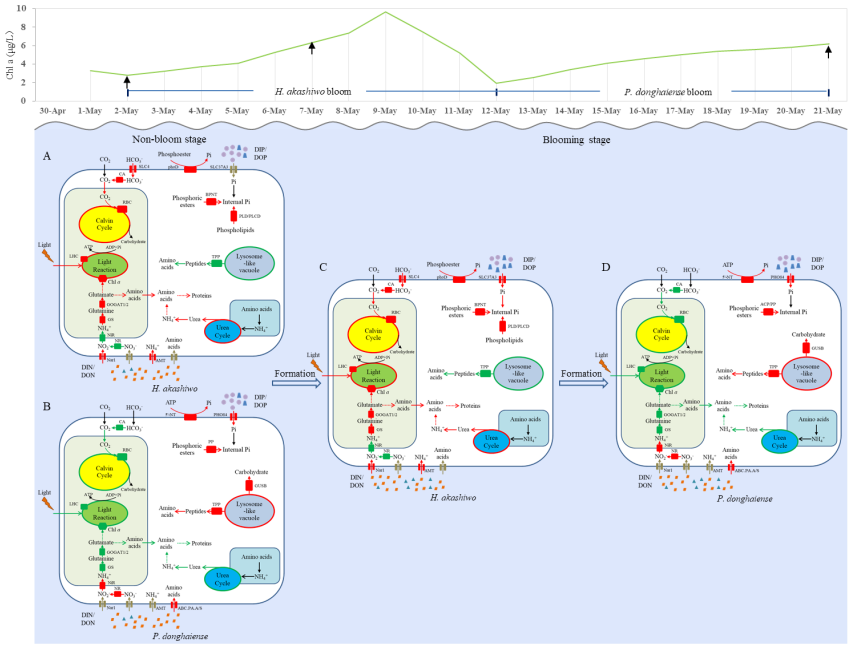

897

898 **FIG 7** Summary of the key molecular events occurring at the *H. akashiwo* and *P. donghaiense* cells during their bloom periods. (A) *H. akashiwo* of the NB sample. (B) *P.*
899 *donghaiense* of the NB sample. (C) *H. akashiwo* of the BHA sample. (D) *P. donghaiense* of the BPD sample. The red and green colors represent higher and lower proportions of
900 metabolic processes and enzymes of one species relative to the other species in the same blooming phase, and the gray color indicates no dection. The arrow represents the sample
901 point. Protein abbreviations are annotated in FIG 5 and 6.